

The Z Charmoniumlike Mesons

Arafat Gabareen Mokhtar^{*1} and Stephen Lars Olsen^{†2}

¹SLAC National Accelerator Laboratory, Stanford, California 94309, USA; ²Seoul National University, KOREA

Abstract

A brief review of the experimental situation concerning the electrically-charged charmoniumlike meson candidates, Z^- , is presented.

Introduction

The Belle Collaboration reported peaks in the $\psi'\pi^-$ [1] and $\chi_{c1}\pi^-$ invariant mass distributions [2] in $B \rightarrow \psi'\pi^-K$ [3] and $B \rightarrow \chi_{c1}\pi^-K$ [4], respectively. If these peaks are meson resonances, they would have a minimal quark substructure of $c\bar{c}d\bar{u}$ and be unmistakably exotic. However, even though the Belle signals have more than 5σ statistical significance, the experimental situation remains uncertain in that none of these peaks have yet been confirmed by other experiments. An analysis by the *BABAR* Collaboration of $B \rightarrow \psi'\pi^-K$ neither confirms nor contradicts the Belle claim for the $Z(4430)^- \rightarrow \psi'\pi^-$ [5]. In the *BABAR* analysis, $B \rightarrow J/\psi\pi^-K$ decays were also studied, and no evidence for $Z(4430)^- \rightarrow J/\psi\pi^-$ was found.

In this paper, we review and compare Belle and *BABAR* results on searches for charged charmoniumlike states. An abbreviated version of this review is contained in Ref. [6].

The Belle observation

Belle's original $Z(4430)^-$ signal [3] is the sharp peak in the $\psi'\pi^-$ invariant mass distribution from $B \rightarrow \psi'\pi^-K$ decays shown in Fig. 1. The Belle analysis is based on a data sample that is equivalent to an integrated luminosity of 605 fb^{-1} . Figure 2 shows the Dalitz plot for $B \rightarrow \psi'\pi^-K$ candidates, where verti-

cal bands for $K^*(892) \rightarrow K\pi^-$ and $K_2^*(1430) \rightarrow K\pi^-$ are evident and the $Z(4430)^-$ shows up as a horizontal band of events between $M_{\psi'\pi^-}^2 = 19$ and $20 \text{ GeV}^2/c^4$. (In the $\psi'\pi^-$ invariant mass distribution of Fig. 1, the K^* bands are suppressed by cuts on the $K\pi^-$ masses [3]).

A binned maximum-likelihood fit to the $\psi'\pi^-$ mass distribution using a Breit Wigner (BW) resonance function for the signal and a polynomial background gives a mass of $M = 4433 \pm 4 \pm 2 \text{ MeV}/c^2$ and total width of $\Gamma = 45_{-13}^{+18} \text{ }_{-13}^{+30} \text{ MeV}$, with estimated statistical significance of more than 6σ . Consistent signals are seen in various subsets of the data: *i.e.* for both the $\psi' \rightarrow \ell^+\ell^-$ ($\ell = e, \text{ or } \mu$) and $\psi' \rightarrow J/\psi\pi^+\pi^-$ ($J/\psi \rightarrow \ell^+\ell^-$) subsamples [3].

A reflection from $K\pi$ dynamics?

Identifying resonant structures in the $\psi'\pi^-$ channel in three-body $B \rightarrow \psi'\pi^-K$ decays has to be done with care because of the possibility that dynamics in the $K\pi^-$ channel can cause mass structures in the $\psi'\pi^-$ invariant mass distribution that have no relation to $\psi'\pi^-$ dynamics. Energy-momentum conservation imposes a tight correlation between the decay angle (θ_{π^-}) in the $K\pi^-$ system [7] and the $\psi'\pi^-$ invariant mass, and this results in $M_{\psi'\pi^-}^2$ being very nearly proportional to $\cos\theta_{\pi^-}$. Consequently, interference between different partial waves in the $K\pi^-$ system can produce peaks in $M_{\psi'\pi^-}$ that are purely “reflections” of structures in $\cos\theta_{\pi^-}$ and have nothing to do with $\psi'\pi^-$ dynamics. However, in the kinematically allowed $K\pi^-$ mass range for $B \rightarrow \psi'\pi^-K$ decay, only S -, P - and D -waves are significant, and this limited set of partial waves can only produce fake $\psi'\pi^-$ mass peaks at a discrete set of mass values.

In the case of the $Z(4430)^-$, the $\psi'\pi^-$ peak mass

^{*}mokhtar@slac.stanford.edu

[†]solsen@hep1.snu.ac.kr

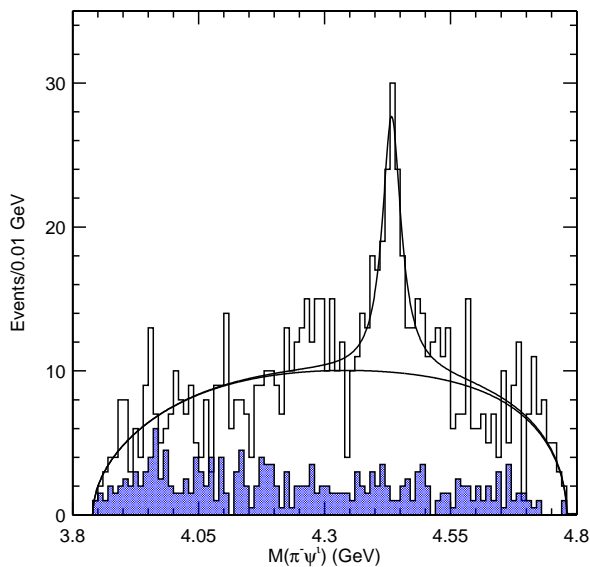


Figure 1: From Belle [3], the $\psi'\pi^-$ invariant mass distribution for $B \rightarrow \psi'\pi^- K$ decays after applying a veto on the $K^*(892)$ and $K_2^*(1430)$. The open histogram shows the data, and the shaded histogram represents the scaled results from the background. The solid curves are the fit results.

corresponds to $\cos\theta_{\pi^-} \simeq 0.25$, and it is not possible to produce a peak near this $\cos\theta_{\pi^-}$ value with any combination of interfering $L = 0, 1$, and 2 partial waves without introducing additional, larger structures at other $\cos\theta_{\pi^-}$ values. This is illustrated in Fig. 3, where the histogram shows the distribution of $\cos\theta_{\pi^-}$ values for a MC sample of $B \rightarrow Z(4430)^- K$, $Z(4430)^- \rightarrow \psi'\pi^-$ events where the $Z(4430)^-$ mass and width closely correspond to Belle’s reported values [3]. The curves in the figure show the results of trying to make a peak at the same location with interfering S -, P - and D -partial waves in the $K\pi^-$ channel. (Here both longitudinally and transversely polarized ψ' ’s are considered, and no attempt is made to restrict the strength of each term to that seen for the S -, P - and D -wave $K\pi^-$ components in the data.) These curves show that although a peak can be made at $\cos\theta_{\pi^-} \simeq 0.25$, it is necessarily accompanied by large enhancements near $\cos\theta_{\pi^-} \simeq \pm 1$. No such structures are evident in the $\psi'\pi^-$ mass plot of Fig. 1.

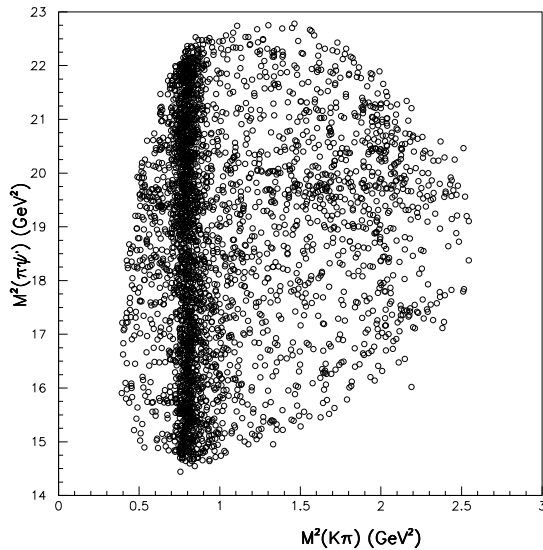


Figure 2: From Belle [3], the $M_{K\pi^-}^2$ (horizontal) vs. $M_{\psi'\pi^-}^2$ (vertical) Dalitz plot distribution for candidate $B \rightarrow \psi'\pi^- K$ events.

The *BABAR* search for the $Z(4430)^-$

BABAR searched [5] for the $Z(4430)^-$ in the decay modes $B \rightarrow \psi\pi^- K$, where $\psi = J/\psi$ or ψ' and $K = K^+$ or K_S^0 . The search was performed using the full *BABAR* data set equivalent to integrated luminosity of 413 fb^{-1} ($455 \times 10^6 B\bar{B}$ candidates) collected at a center-of-mass energy of 10.58 GeV. The *BABAR* search covered two additional decay modes ($B \rightarrow J/\psi\pi^- K$) that were not considered in the Belle study. The J/ψ modes contain about six times (see Table II in Ref. [5]) more data than those with the ψ' and provide a powerful, high statistics tool for understanding the background. The Dalitz plots for the four decay modes are shown in Fig. 4. The $K\pi^-$ mass distribution shows a clear $K^*(892)$ signal in all decay modes, and a visible $K_2^*(1430)$ signal in the modes with a J/ψ but less significant in the modes with ψ' . Since the $K\pi^-$ system dominates the Dalitz plot, the *BABAR* Collaboration studied the $K\pi^-$ mass distribution and the angular dependence. Similar contributions from the different wave intensities are obtained in the modes with K_S^0 and K^+ (see Table III in Ref. [5]) and, therefore, the modes with K_S^0 and K^+ are combined. The $K\pi^-$ mass distributions are fitted

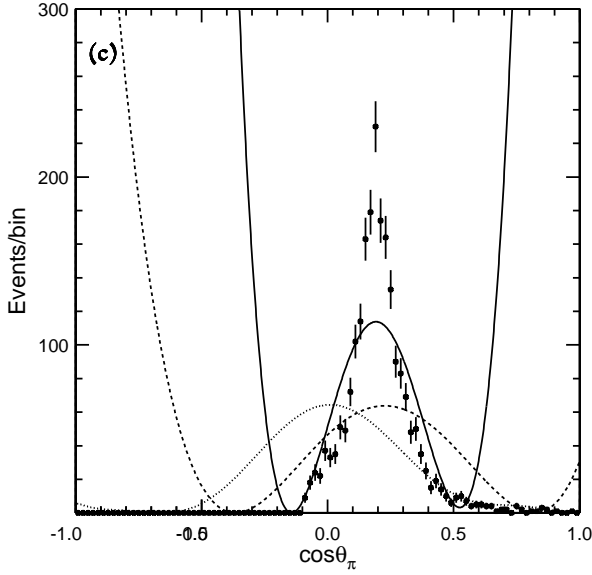


Figure 3: From Ref. [8], the histogram shows the $\cos \theta_{\pi^-}$ distribution for a MC-generated $\psi' \pi^-$ resonance with $M = 4.43 \text{ GeV}/c^2$ and $\Gamma = 0.05 \text{ GeV}$. The curves show the results of attempts to produce a peak in the vicinity of the data with interfering S -, P - and D -waves in the $K \pi^-$ channel.

with the S -, P -, and D -wave intensities as shown in Fig. 5. Good fits to the data are obtained. The study of the angular dependence shows a clear asymmetry in $\cos \theta_K$, where θ_K is the angle between the Kaon and ψ meson in the $K \pi^-$ rest frame (see Figs. 12 and 13 in Ref. [5]).

The *BABAR* mass resolution at the $Z(4430)^-$ mass is 7 (4) MeV/c^2 for the modes with J/ψ (ψ') (see Fig. 6 in Ref. [5]). Each event is efficiency corrected, and the conclusions are based on distributions obtained after background subtraction. The average efficiency varies slightly as a function of the $K \pi^-$ mass but can differ significantly between the different ψ decay modes (see Fig. 7 in Ref. [5]), however there are significant variations in efficiency with $\cos \theta_K$ for certain regions of $K \pi^-$ mass (see Fig. 36 in Ref. [5]).

The comparison between the $\psi \pi^-$ mass distribution and the relevant $K \pi^-$ reflection was performed (see section 9 in Ref. [5]). This comparison is essential to investigate the need for a $Z(4430)^-$ signal above the $K \pi^-$ reflection. Following the five $K \pi^-$ regions (see section 10.D in Ref. [5]) defined in the

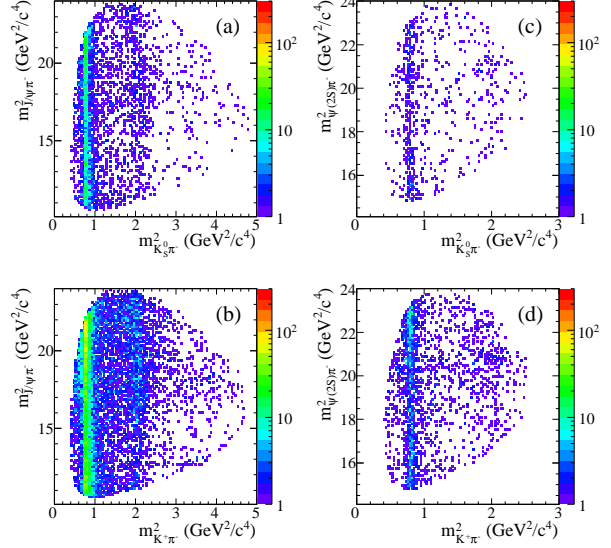


Figure 4: From *BABAR* [5], the $m_{\psi \pi^-}^2$ versus $m_{K \pi^-}^2$ Dalitz plots for the final samples in the decay modes (a) $B^- \rightarrow J/\psi \pi^- K_S^0$, (b) $B^0 \rightarrow J/\psi \pi^- K^+$, (c) $B^- \rightarrow \psi' \pi^- K_S^0$, and (d) $B^0 \rightarrow \psi' \pi^- K^+$.

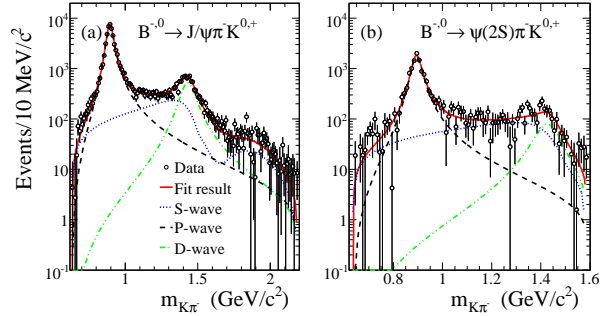


Figure 5: From *BABAR* [5], the fit results to the $K \pi^-$ mass distributions for the combined $K \pi^-$ charge configurations (a) $B^{-,0} \rightarrow J/\psi \pi^- K^{0,+}$ and (b) $B^{-,0} \rightarrow \psi' \pi^- K^{0,+}$. The open dots show the data, and each curve represents different fit contribution, as indicated.

Belle analysis [3], the projection is implemented in each $K \pi^-$ interval as shown in Fig. 6. In each figure, a comparison (not a fit) between the data and the $K \pi^-$ reflection is shown. Note that only one normalization factor for the $K \pi^-$ regions is used for each ψ mode. The $K \pi^-$ reflections onto the $\psi \pi^-$ mass distributions describe well the data, with a small statistical fluctuation at $m_{K \pi^-} < 0.795 \text{ GeV}/c^2$. The

$\psi\pi^-$ mass distribution and the overall $K\pi^-$ projection are shown in Fig. 7. No significant evidence for $Z(4430)^-$ has been obtained. The $K\pi^-$ projection onto the $\psi\pi^-$ mass distribution is used as a non-peaking background. With such a background shape and a BW function for a $Z(4430)^-$ signal, a signal is obtained for the overall $K\pi^-$ region, but with shifted mass value. A similar small signal is obtained in the $K^*(892)$ and $K_2^*(1430)$ combined regions. A $\sim 2\sigma$ peak is obtained when the $K^*(892)$ and $K_2^*(1430)$ regions are vetoed. No (or a negative) signal for $Z(4430)^- \rightarrow J/\psi\pi^-$ was found.

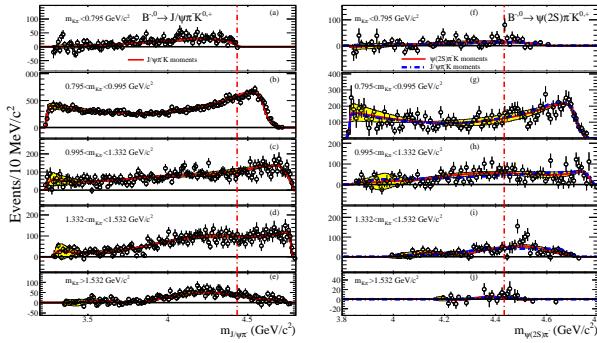


Figure 6: From *BABAR* [5], the $\psi\pi^-$ mass distributions in different regions of $K\pi^-$ mass for (a-e) $B^{-,0} \rightarrow J/\psi\pi^- K^{0,+}$, and (f-j) $B^{-,0} \rightarrow \psi'\pi^- K^{0,+}$; the open dots represent the data, and the solid curves and shaded bands are due to the $K\pi^-$ reflections in the different $\psi\pi^-$ mass intervals, using the same overall normalization constant. In (f-j), the dot-dashed curves are obtained using $K\pi^-$ normalized moments for $B^{-,0} \rightarrow J/\psi\pi^- K^{0,+}$, instead of those from $B^{-,0} \rightarrow \psi'\pi^- K^{0,+}$; the vertical lines indicate $m_{\psi\pi^-} = 4.433 \text{ GeV}/c^2$.

Although the Belle Collaboration used a data sample equivalent to 1.46 times that of *BABAR*'s, because of different selection criteria *BABAR* has more events per fb^{-1} . A direct comparison between the two $m_{\psi\pi^-}$ distributions is shown in Fig. 8. For comparison purposes, the *BABAR* distribution is not corrected for efficiency, however both Belle and *BABAR* distributions are background subtracted and shown in Fig. 8(a) and Fig. 8(b), respectively. The *BABAR* distribution is scaled up by the factor 1.18 in order to normalize to the Belle data between the crosshatched regions of Fig. 8(c). The difference plot is shown in

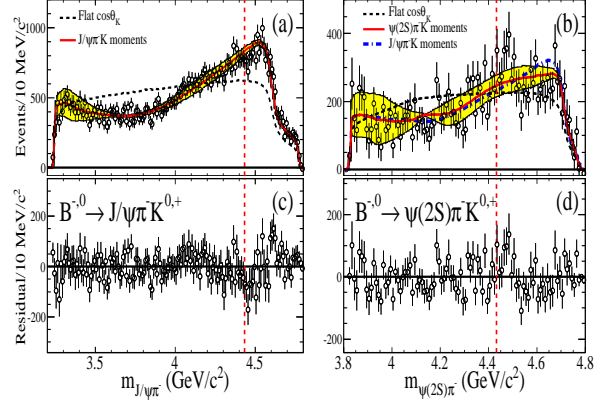


Figure 7: From *BABAR* [5], the $\psi\pi^-$ mass distributions for the combined decay modes (a) $B^{-,0} \rightarrow J/\psi\pi^- K^{0,+}$ and (b) $B^{-,0} \rightarrow \psi'\pi^- K^{0,+}$. The points show the data (integrated over all $K\pi^-$ regions) after efficiency correction and background subtraction. The dashed curves show the $K\pi^-$ reflection for a flat $\cos\theta_K$ distribution, while the solid curves show the result of $\cos\theta_K$ when accounting for the angular dependence (see Sec. 9 in Ref. [5]). The shaded bands represent the effect of statistical uncertainty on the normalized moments. In (b), the dot-dashed curve indicates the effect of weighting with the normalized $J/\psi\pi^- K$ moments. The dashed vertical lines indicate the value of $m_{\psi\pi^-} = 4.433 \text{ GeV}/c^2$. In (c) and (d), we show the residuals (data-solid curve) for (a) and (b), respectively.

Fig. 8(c) where errors have been combined in quadrature; here $\chi^2/NDF = 54.7/58$, which indicates that the two samples are statistically equivalent.

Belle's Dalitz analysis of $B \rightarrow \psi'\pi^- K$

After the *BABAR* Collaboration did not confirm the $Z(4430)^- \rightarrow \psi'\pi^-$ mass peak in their analysis of $B \rightarrow \psi'\pi^- K$ decays [5], the Belle Collaboration performed a reanalysis [9] of their data that took detailed account of possible reflections from the $K\pi^-$ channel. Specifically, they modeled the $B \rightarrow \psi'\pi^- K$ process as the sum of two-body decays $B \rightarrow \psi' K_i^*$, where K_i^* denotes all of the known $K^* \rightarrow K\pi^-$ resonances that are kinematically accessible, and both with and with-

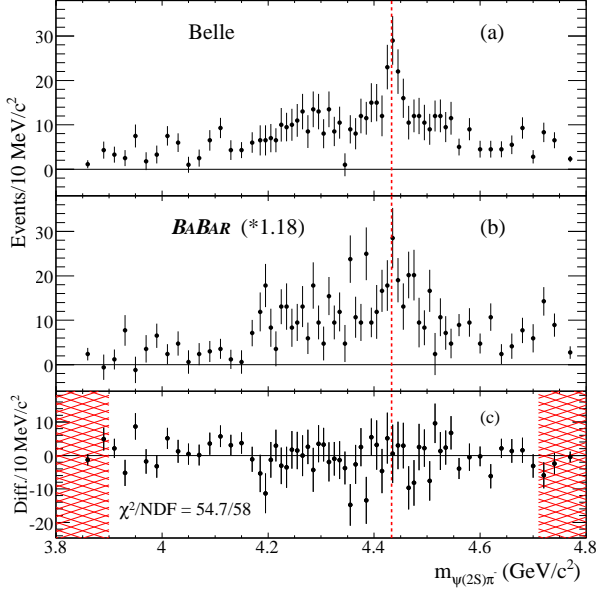


Figure 8: From *BABAR* [5], (a) The Belle $m_{\psi'\pi^-}$ distribution after background subtraction; (b) the equivalent *BABAR* $m_{\psi'\pi^-}$ distribution obtained after scaling due to different luminosities. (c) The difference between the $m_{\psi'\pi^-}$ distributions. The crosshatched area represents the exclusion region for the normalization procedure. The vertical-dashed line indicates $m_{\psi'\pi^-} = 4430 \text{ MeV}/c^2$.

out a $B \rightarrow Z(4430)^- K$ component. The results of this analysis, confirm the basic conclusions of Belle’s initial publication [3].

Figure 9 shows the $\psi'\pi^-$ mass distribution in different $K\pi^-$ intervals as obtained from the Dalitz-plot analysis by the Belle Collaboration [9]. In the region between the $K^*(892)$ and the $K_2^*(1430)$ ($0.982 < m_{K\pi} < 1.332 \text{ GeV}/c^2$, Fig. 9(c)), a $Z(4430)^-$ peak is present. The data points in Fig. 10 show $M_{\psi'\pi^-}^2$ Dalitz plot projections with the prominent K^* bands removed (as in Fig. 1) compared with the results of the fit with no $Z(4430)^-$ resonance, shown as a dashed histogram, and that with a $Z(4430)^-$ resonance, shown as the solid histogram. The fit with the $Z(4430)^-$ is favored over the fit with no $Z(4430)^-$ by 6.4σ . The fitted mass, $M = 4443_{-12}^{+15} \text{ MeV}/c^2$, agrees within the systematic errors with the earlier Belle result; the fitted width, $\Gamma = 107_{-43}^{+86} \text{ MeV}$, is larger, but also within the analysis’ systematic er-

rors of the previous result. In the default fit, the $Z(4430)^-$ resonance was assumed to have zero spin. Variations of the fit that included a $J = 1$ assignment for the $Z(4430)^-$ as well as models that included additional, hypothetical $K^* \rightarrow K\pi^-$ resonances with floating masses and widths, and radically different parameterizations of the $K\pi^-$ S -wave amplitude do not change the conclusions. The product branching fraction from the Dalitz fit: $\mathcal{B}(B^0 \rightarrow Z(4430)^- K) \times \mathcal{B}(Z(4430)^- \rightarrow \psi'\pi^-) = (3.2_{-0.9}^{+1.8} \text{ }_{-1.6}^{+9.6}) \times 10^{-5}$ is not in strong contradiction with the *BABAR* 95% C.L. upper limit of 3.1×10^{-5} [5].

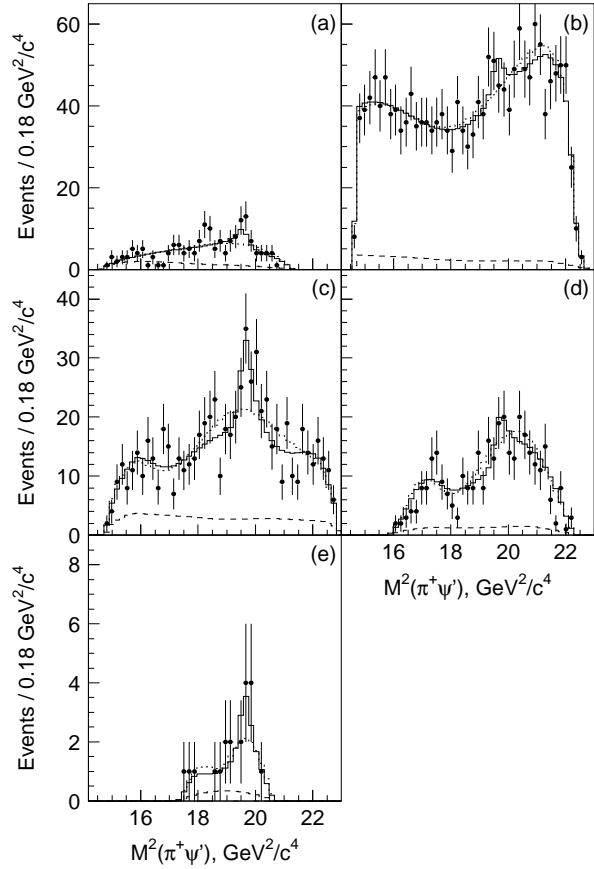


Figure 9: From Belle [9], $M_{\psi'\pi^-}^2$ projections for $M_{K\pi}$ bands: (a) below the $K^*(892)$; (b) at the $K^*(892)$; (c) between the $K^*(892)$ and the $K_2^*(1430)$; (d) at the $K_2^*(1430)$; and (e) above the $K_2^*(1430)$. The dots show the data, the solid (dotted) histograms are the results for the model with (without) a single $\psi'\pi^-$ state, and the dashed histograms are the background contaminations.

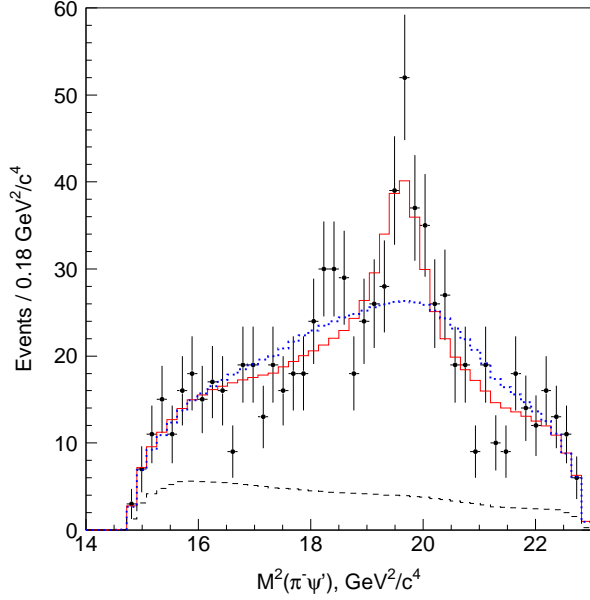


Figure 10: From Belle [9], the $M_{\psi'\pi^-}^2$ projection of the Dalitz plot with the K^* bands removed is shown as data points. The histograms show the corresponding projections of the fits with and without a $Z(4430)^- \rightarrow \psi'\pi^-$ resonance term.

Belle's two Z peaks in the $\chi_{c1}\pi^-$ channel

In addition to the $Z(4430)^-$, Belle has presented results of an analysis of $B \rightarrow \chi_{c1}\pi^- K$ decays that require two resonant states in the $\chi_{c1}\pi^-$ channel [4]. The $M_{K\pi^-}^2$ vs. $M_{\chi_{c1}\pi^-}^2$ Dalitz plot, shown in Fig. 11, shows vertical bands of events corresponding to $K^*(892) \rightarrow K\pi^-$ and $K_2^*(1430) \rightarrow K\pi^-$, plus a broad horizontal band near $M_{\chi_{c1}\pi^-}^2 \simeq 17.5 \text{ GeV}^2/c^4$, indicating a possible resonance in the $\chi_{c1}\pi^-$ channel. In this case, this horizontal band corresponds to $\cos\theta_{\pi^-} \simeq 0$, a location where interference between partial waves in the $K\pi^-$ channel can produce a peak and, thus, a detailed Dalitz analysis is essential.

For $B \rightarrow \chi_{c1}\pi^- K$, the kinematically allowed mass range for the $K\pi^-$ system extends beyond the $K_3^*(1780)$ F -wave resonance and S -, P -, D - and F -wave terms for the $K\pi^-$ system are included in the model. The fit with a single resonance in the $Z^- \rightarrow \chi_{c1}\pi^-$ channel is favored over a fit with only K^* resonances and no Z^- by more than 10σ . Moreover, a fit with two resonances in the $\chi_{c1}\pi^-$ channel is favored over the fit with only one Z^- resonance by

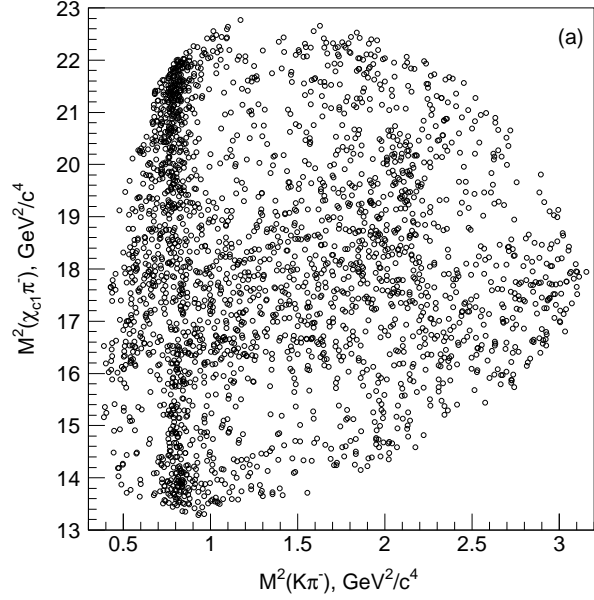


Figure 11: From Belle [4], the $M_{K\pi^-}^2$ (horizontal) vs. $M_{\chi_{c1}\pi^-}^2$ (vertical) Dalitz plot distribution for candidate $B \rightarrow \chi_{c1}\pi^- K$ events.

5.7σ . The fitted masses and widths of these two resonances are: $M_1 = 4051 \pm 14_{-41}^{+20} \text{ MeV}/c^2$ and $\Gamma_1 = 82_{-17}^{+21} {}_{-22}^{+47} \text{ MeV}$ and $M_2 = 4248_{-29}^{+44} {}_{-35}^{+180} \text{ MeV}/c^2$ and $\Gamma_2 = 177_{-39}^{+54} {}_{-61}^{+316} \text{ MeV}$. Here also, variations of the fit that use a $J = 1$ assignment for the Z^- states and models that include additional, hypothetical $K^* \rightarrow K\pi^-$ resonances with floating masses and widths, and different parameterizations of the $K\pi^- S$ -wave amplitude do not change the conclusions.

The product branching fractions for $B \rightarrow Z^-(\rightarrow \chi_{c1}\pi^-)K$ have central values similar to that for the $Z(4430)^-$ but with large errors. Figure 12 shows the $M_{\chi_{c1}\pi^-}$ projection of the Dalitz plot with the K^* bands excluded and the results of the fit with no $Z^- \rightarrow \chi_{c1}\pi^-$ resonances and with two $Z^- \rightarrow \chi_{c1}\pi^-$ resonances.

Summary

If the peaks reported by Belle in the $\psi'\pi^-$ and $\chi_{c1}\pi^-$ channels are in fact meson resonances, they would be “smoking guns” for exotics. It is therefore important that the Belle results are confirmed (or refuted) by other experiments. Both the *BABAR* and Belle $\psi'\pi^-$ analyses could benefit from additional

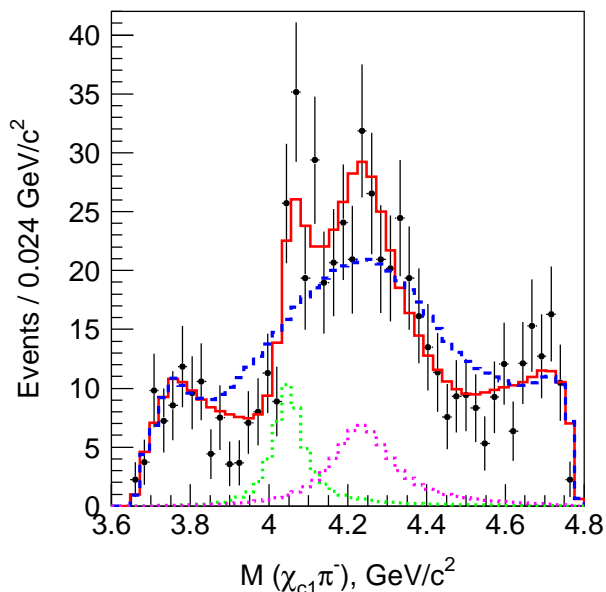


Figure 12: From Belle [4], the data points show the $M_{\chi_{c1}\pi^-}$ projection of the Dalitz plot with the K^* bands removed. The histograms show the corresponding projections of the fits with and without the two $Z \rightarrow \chi_{c1}\pi^-$ resonance terms.

statistics. However, both experiments have completed data taking and the *BABAR* analysis used their complete dataset while the Belle analysis used about 75% of their final total data sample. Approximately 3 ab^{-1} of integrated luminosity would be necessary to bring the $\psi'\pi^-$ sample to the statistical level of *BABAR*'s current $J/\psi\pi^-$ sample, and this amount of data will not be available until the operation of one of the Super-*B* factories, which will not happen for at least a few years. In the meantime, it would be valuable if *BABAR* performed a search for the $Z_1(4050)^-$ and $Z_2(4250)^-$ in the $\chi_{c1}\pi^-$ channel and Belle reproduced *BABAR*'s study of the $J/\psi\pi^-$ channel using the existing data sets. The D0 and CDF experiments at the Tevatron have data on hand that could be used to carry out searches for inclusive production of the $Z(4430)^-$ and we hope that results will be available from them in the near future.

Acknowledgment

The work of Arafat Gabareen Mokhtar is supported by the US Department of Energy, Division

of High Energy Physics, Contract DE-AC02-76-SF00515. The work of Stephen Lars Olsen is supported by the WCU program of the Korean Ministry of Education, Science and Technology (grant number R32-2008-000-10155-0).

References

- [1] The notations ψ' and $\psi(2S)$ are used for the same charmonium state of $\psi(3686)$.
- [2] The inclusion of charge-conjugate modes is always implied. Also, when two errors are presented, the first one is always statistical and the second systematic.
- [3] S.-K. Choi *et al.* (Belle Collaboration), *Phys. Rev. Lett.* **100**, 142001 (2008).
- [4] R. Mizuk *et al.* (Belle Collaboration), *Phys. Rev. D* **78**, 072004 (2008).
- [5] B. Aubert *et al.* (*BABAR* Collaboration), *Phys. Rev. D* **79**, 112001 (2009).
- [6] N. Brambilla *et al.* (Quark Working Group), arXiv:1010.5827, to be published in European Journal of Physics C.
- [7] θ_{π^-} is the angle between the π^- and the negative of the ψ' direction in the $K\pi^-$ rest frame.
- [8] S. L. Olsen, talk at the 2009 International Workshop on Charm Physics, Leiman Germany, May 2009; arXiv:0909.2713.
- [9] R. Mizuk *et al.* (Belle Collaboration), *Phys. Rev. D* **80**, 031104 (2009).